Proceedings of CHT-12
ICHMT International Symposium on Advances in Computational Heat Transfer

July 1-6, 2012, Bath, England

CHT12-MP09

ADVANCEMENT IN TURBULENT SPRAY MODELLING: THE EFFECT OF INTERNAL TEMPERATURE GRADIENT IN DROPLETS

A.Yu. Snegirev[1§], V.A. Talalov[1], A.S. Tsoi[1], S.S. Sazhin[2], C. Crua[2]
[1] Department of Thermal Physics, Saint-Petersburg State Polytechnic University, Polytechnicheskaya, 29, Saint-Petersburg 195251, Russia
[2] Sir Harry Ricardo Laboratories, School of Computing, Engineering and Mathematics, University of Brighton, Brighton BN2 4GJ, U.K.
[§]Correspondence author. Email: a.snegirev@phmf.spbstu.ru

ABSTRACT. Two simple and yet sufficiently accurate approaches to predict surface temperature of a vaporizing droplet (higher order polynomial approximation and the heat balance integral method) are proposed. Being computationally inexpensive these approaches are tested as candidates for use in high-resolution LES spray modelling. Robust and efficient numerical algorithm for solving inherently stiff equations of droplet heating and evaporation has been developed. Robustness and computational efficiency of the proposed algorithm is achieved by use of unconditionally stable strongly implicit integration scheme and appropriate adaptation of the time step. The above methodology has been implemented in CFD spray model included in the in-house Fire3D code. The spray model has been applied to replicate three essentially different experimental scenarios in which turbulent sprays of water, acetone, and diesel fuel were investigated. Reasonable agreement has been demonstrated for predicted and measured droplet sizes and velocities as well as for the spray tip penetration dynamics. New numerical algorithms used to calculate surface temperatures of evaporating droplets with non-uniform internal temperature did not incur observable increase of CPU time in turbulent spray simulations.

INTRODUCTION

Turbulent sprays occurring in engineering applications and environmental phenomena are very versatile due to various liquids dispersed, different mechanisms of liquid atomization, wide range of droplet sizes and discharge velocities, as well as of ambient gas temperatures, pressures and compositions. As such, a unified approach is required which could make the spray model applicable to different sprays developing in different external conditions, including those situations where internal temperature non-uniformity affects evaporation dynamics. Another challenge is imposed by growing spatial and transient resolution requirements in turbulent flow simulations which also imply a very large amount of computational particles considered. To meet the above requirements, the advancements are introduced in this work into the droplet heating and evaporation submodel allowing for the internal temperature gradient by means of simple and robust approach.

Although uniformity of liquid temperature inside a vaporizing droplet (the infinite conductivity concept) is conventionally assumed in most of the existing spray models, its limitations were highlighted in a number of papers, e.g. Law and Sirignano [1977], Sirignano [1983], Aggarwal *et al.* [1984], Bertoli and Migliaccio [1999], Sazhin *et al.* [2005] among others. In the above works, an

observable difference has been demonstrated in evaporation rates predicted by assuming finite and infinite liquid conductivity. Such a difference was observed at the initial transient stage of droplet heating in a hot gas environment. It has been recognised that consideration of heat transfer inside the droplet is closely coupled with liquid circulation driven by the shear stress developing at the surface of moving droplet.

Direct resolution of temperature field in a circulating liquid requires numerical solving of Navier-Stokes equations in every droplet which is not affordable in spray modelling. An approximate solution to this problem can be obtained using the effective conductivity model in which liquid circulation is accounted for by appropriately increased thermal conductivity of the liquid. Such an effective thermal conductivity is set to be a function of liquid Peclet number which is formulated in terms of estimated liquid velocity at the droplet surface, see [Abramson and Sirignano, 1989]. Within the framework of the effective conductivity concept, the internal heat transfer model is reduced to the heat conductivity equitation only; despite of this, exact (numerical or analytical) solution to this equation in every droplet imposes significant and hardly affordable computational cost.

Therefore, attempts have been made to develop approximate models which take temperature non-uniformity in vaporizing droplets into account. To allow for the internal heat and mass transfer inside evaporating droplet, an approximate model has been developed by Renksizbulut et al. [1992] who described droplet temperature field by two values of: surface temperature and droplet core temperature. It was further assumed that due to the heat transfer the difference between these quantities is proportional to the heat flux accepted by the droplet at its surface. The above assumption is equivalent to setting Nusselt-like number calculated at the liquid side of the droplet surface to be constant. In fact, this assumption is a consequence of establishing quasi-steady temperature field inside the droplet, which is clearly illustrated by the first of Eqs (22) derived below using quasi-steady parabolic approximation. Not surprisingly, such an approximation is not valid at early times of droplet heating (or cooling); this issue is discussed in detail in this paper.

Two-temperature approach can be derived more rigorously if a particular functional form of internal temperature distribution is assumed. This is the idea of parabolic approximation when the radial temperature distribution is assumed to be second order polynomial as suggested by Dombrovsky and Sazhin [2003] (note, that this approximation was earlier used for modelling diffusion of lithium in spherical particles of active material, *e.g.* by Subramanian *et al.* [2001]). The droplet core temperature is formally defined as volume-averaged temperature which is coupled (via heat balance ODE) to droplet surface temperature and the heat flux received by the liquid. More recently, two-temperature approach was applied in the model by Balasubramanyam *et al.* [2007]. However, instead of using constant value for the proportionality coefficient between the surface and core temperatures, this coefficient was calculated by Balasubramanyam *et al.* [2007] from thermal resistance of thermal boundary layer with effective thermal diffusivity, a_{eff}, estimated for (presumably) fully developed turbulent liquid flow inside the droplet. Thickness of the thermal boundary layer was calculated as $\sqrt{\pi a_{eff} \Delta t}$, which is questionable when its value is comparable to the droplet radius. Furthermore, the time scale, Δt, is set equal to the evaporation sub-cycle time step which introduced another source of a possible inaccuracy to the model. Nevertheless, such a model was successfully applied by Balasubramanyam and Chen [2008] to predict evaporating spray penetration in a high-speed cross-flow. Use of the above finite-conductivity model improved agreement of the predictions with the measurements, although its effect appeared to be comparable to (or even weaker than) the effect of the error introduced by the drag coefficient. It is difficult to extend this conclusion to other conditions of spray development in which the effect of the internal temperature gradient might be important. Similar two-temperature model and thermal boundary layer concept were utilized by Ra and Reitz [2009] who

calculated effective thermal diffusivity using liquid circulation factor (the latter being a function of Peclet number), which was derived by Abramson and Sirignano [1989].

Clearly, a more universal and more consistent model is required which should also be as simple as possible to minimize computational cost. Combination of model simplicity and capability to accurately predict droplet surface temperature is crucial for efficient use in a CFD spray model which deals with a very large number of droplets. In this work we propose two approximate approaches to determine droplet surface temperature taking internal temperature non-uniformity into account. In this paper, both approaches, high order polynomial approximation and the integral heat balance method, are formally derived using the effective conductivity concept (thereby allowing for the internal liquid circulation) and shown to be accurate at all times, including initial transient stage of droplet heating. These approaches have been incorporated in the in-house LES-based spray model which has been validated against three evaporating liquid sprays of water, acetone and diesel fuel.

DROPLET HEATING AND EVAPORATION MODELLING

The approach developed by Abramzon and Sirignano [1989] is used here to simulate droplet heating and evaporation. Model details can be found in the original and subsequent papers (e.g. by Sazhin [2006]) and are not repeated here. Droplet heat balance is determined by three components, which include heat spent for liquid vaporization,

$$Q_{vap} = \Delta h_{vap}\left(T_s\right)\dot{m}, \tag{1}$$

and convective heat flux received by the droplet,

$$Q_{conv} = \pi d \mathrm{Nu}^{*}\left(\ln\left(1+B_T\right)/B_T\right)\lambda_g\left(T_g - T_s\right), \tag{2}$$

where $\Delta h_{vap}\left(T_s\right)$ is the heat of vaporization at droplet surface temperature T_s, m and d are the droplet mass and diameter, λ_g and T_g is the thermal conductivity and temperature of ambient gas, Nu^{*} is vaporization-modified Nusselt number, $B_T = c_{P,vap}\left(T_g - T_s\right)\Big/\left(\Delta h_{vap}\left(T_s\right) - Q_d/\dot{m}\right)$, and Q_d is the heat flux received by the droplet.

The third component is radiative heat flux which is evaluated for non-transparent droplets:

$$Q_{rad} = -\pi d^2 \varepsilon\sigma\left(T_s^4 - T_{rad}^4\right). \tag{3}$$

In Eq. (3), T_{rad} is the radiative ambient temperature which is determined as $T_{rad} = \left(G/4\sigma\right)^{1/4}$, where G is the incident radiation obtained from radiative transfer model applied in the ambient gas. In this work, the Monte Carlo approach is used jointly with the weighted sum of gray gases model as described by Snegirev [2004]. Droplet transparency for infrared radiation is neglected based on the conclusions by Sirignano [2010] that radiative transfer inside the droplet is of secondary importance compared to heat transfer by thermal conductivity and liquid circulation.

Combination of the heat spent for liquid vaporization and convective heat flux received by the droplet is formulated as

$$Q_{conv} + Q_{vap} = -c_l m\left(T_s - T_{wb}\right)/\tau_{conv}, \tag{4}$$

where T_{wb} is the equilibrium surface temperature (wet bulb temperature), τ_{conv} is the convective time scale (characteristic of surface temperature relaxation to the equilibrium value). According to Eqs (1), (2) and (4), convective time scale τ_{conv} is

$$\tau_{conv} = \frac{c_l m\left(T_s - T_{wb}\right)}{\pi d \mathrm{Nu}^* \left(\ln\left(1+B_T\right)/B_T\right)\lambda_g \left(T_s - T_g\right) - \Delta h_{vap}\dot{m}}. \quad (5)$$

Wet bulb temperature obeys the thermal equilibrium equation

$$Q_{conv}\left(T_{wb}\right) + Q_{vap}\left(T_{wb}\right) = 0. \quad (6)$$

Calculated wet bulb temperature for acetone and water is compared in Fig. 1 with the empirical data available.

To evaluate thermal properties and transport coefficients, conventional 1/3 rule is applied, and the reference temperature and vapour mass fractions are determined as $T^{ref} = T_s + \left(T_g - T_s\right)/3$ and $Y_{vap}^{ref} = Y_{vap,s} + \left(Y_{vap,g} - Y_{vap,s}\right)/3$ respectively. However, it was found that this approach produced underestimated wet bulb temperature for water and acetone at high ambient temperatures. The best agreement (shown in Fig. 1) with the empirical data was obtained when the exception was made for the vapour diffusion coefficient, and the latter was calculated at droplet surface temperature. The same approach is used in all the simulations shown in this work.

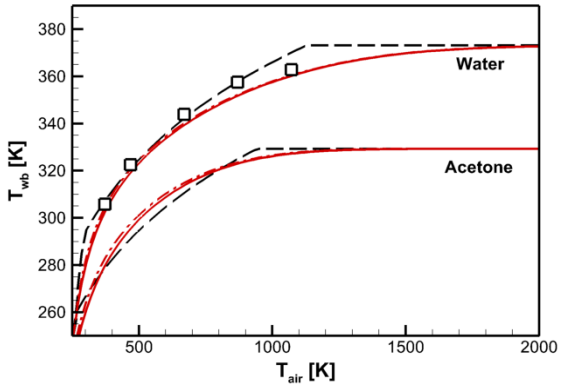

Fig. 1. Wet bulb temperature as a function of ambient air temperature. Solid and dash-dot lines – simulations with the Clausius-Clapeyron and Antoine equations, respectively, dashed lines – empirical correlation by Miller *et al.* [1998], symbols – measurements by Yuen and Chen [1976]

Temperature dependencies of thermal properties and transport coefficients are taken from a number of sources, including books by Reid *et al.* [1987], Dean [1999], Bird et al. [2002].

When the thermal radiation is taken into account, Eq. (3) is linearized:

$$Q_{rad} = -c_l m \frac{T_s - T_{rad}}{\tau_{rad}}, \text{ where } \tau_{rad} = \frac{c_l m}{\pi d^2 \varepsilon \sigma \left(T_s^2 + T_{rad}^2\right)\left(T_s + T_{rad}\right)}. \quad (7)$$

Total heat flux received by the droplet is therefore

$$Q_d = Q_{conv} + Q_{vap} + Q_{rad} = -c_l m \frac{T_s - T_{wb}}{\tau_{conv}} - c_l m \frac{T_s - T_{rad}}{\tau_{rad}} = -c_l m \frac{T_s - T_{eq}}{\tau_{eq}}, \quad (8)$$

where

$$T_{eq} = \frac{T_{wb}/\tau_{conv} + T_{rad}/\tau_{rad}}{1/\tau_{conv} + 1/\tau_{rad}} \text{ and } \frac{1}{\tau_{eq}} = \frac{1}{\tau_{conv}} + \frac{1}{\tau_{rad}}. \quad (9)$$

In the absence of thermal radiation $Q_{rad} = 0$, $T_{eq} = T_{wb}$ и $\tau_{eq} = \tau_{conv}$.

HEAT TRANSFER INSIDE VAPORIZING DROPLET

Internal heat transfer is described by the heat conductivity equation

$$c_l \rho_l \frac{\partial T}{\partial t} = \frac{1}{r^2}\frac{\partial}{\partial r} r^2 \lambda_{l,eff} \frac{\partial T}{\partial r}, \tag{10}$$

where $c_l = c_l(T)$, $\rho_l = \rho_l(T)$ is the liquid specific heat and density, $\lambda_{l,eff}$ is the effective conductivity coefficient that approximately takes liquid circulation into account (see [Abramzon and Sirignano, 1989]). The above equation is solved subject to boundary conditions:

$$-\lambda_{l,eff}\left(\partial T/\partial r\right)_{r=0} = 0, \tag{11}$$

$$-\lambda_{l,eff}\left(\partial T/\partial r\right)_{r=R(t)} = q_s, \tag{12}$$

where $q_s = -\left(Q_{conv} + Q_{vap} + Q_{rad}\right)/4\pi R^2$. Numerical stability can be improved if boundary condition (12) is formulated as

$$-\lambda_l\left(\partial T/\partial r\right)_{r=R(t)} = \alpha_{eff}\left(T_s - T_{eq}\right), \tag{13}$$

where α_{eff} is the effective heat transfer coefficient, T_{eq} is the equilibrium temperature given by Eq. (9).

By integrating Eq. (10) over the droplet volume, the heat balance equation is obtained:

$$c_l m \frac{d\overline{T}}{dt} = Q_{conv}(T_s) + Q_{vap}(T_s) + Q_{rad}(T_s) - \frac{dm}{dt} c_l\left(\overline{T} - T_s\right), \tag{14}$$

where volume-averaged temperature, $\overline{T}$, is defined by

$$\overline{T} = \frac{3}{R^3}\int_0^{R(t)} T(r) r^2 dr. \tag{15}$$

The last term in Eq. (14) can be absorbed by the vaporization term: $Q^*_{vap}(T_s) = \left(\Delta h_{vap}(T_s) - c_l\left(\overline{T} - T_s\right)\right)\dot{m} = \Delta h^*_{vap}(T_s)\dot{m}$. For most liquids $\overline{T} - T_s = \mathrm{O}(10\ \mathrm{K})$, $c_l = \mathrm{O}(10^3\ \mathrm{J/(kg{\cdot}K)})$, $\Delta h_{vap} = \mathrm{O}(10^6\ \mathrm{J/kg})$ and $c_l\left|\overline{T} - T_s\right|/\Delta h_{vap} = \mathrm{O}(10^{-2}) << 1$.

To allow for the dependence of evaporating droplet radius on time, the spatial coordinate in Eq. (10) is transformed as $x = r/R(t)$, and Eq. (10) is rewritten as

$$c_l \rho_l\left(\frac{\partial T}{\partial t} + v\frac{\partial T}{\partial x}\right) = \frac{1}{x^2}\frac{1}{R}\frac{\partial}{\partial x} x^2 \lambda_{l,eff}\frac{1}{R}\frac{\partial T}{\partial x}, \tag{16}$$

where $v = -x\dot{R}/R$ is the displacement speed of transformed coordinate system relative to the old one.

In the subsequent sections, three approximate methods allowing for the internal temperature gradient are described and compared to grid-independent ("exact") numerical solution of Eq. (16).

Parabolic approximation. Temperature distribution inside the droplet is approximated by the second order polynomial (for example, see Dombrovsky and Sazhin [2003], Subramanian *et al.* [2001]):

$$T(r) = c_0 + c_2\left(r/R\right)^2. \tag{17}$$

Quasi-steady profile (17) is assumed to be established immediately, and the initial transient period is ignored. Formation of parabolic profile can be demonstrated analytically when a spherical body of fixed size is heated by the external heat flux, q_s = const. Provided thermal properties are unchanged, exact solution to Eq. (10) with boundary conditions (11), (12) and uniform initial temperature distribution $t = 0$, $T = T_0$ is:

$$T(r,t) = T_0 - \frac{q_s R}{\lambda_{l,eff}}\left(3\frac{a_{l,eff}}{R^2}t - \frac{3}{10}\left(1 - \frac{5}{3}\left(\frac{r}{R}\right)^2\right) - \sum_{n=1}^{\infty} A_n \exp\left(-\gamma_n^2 \frac{a_{l,eff}}{R^2}t\right)\right), \tag{18}$$

where $a_{l,eff} = \lambda_{l,eff}/c_l\rho_l$ is the thermal diffusivity, $A_n = \left(2/\gamma_n^2\cos(\gamma_n)\right)\left(\sin(\gamma_n r/R)/(\gamma_n r/R)\right)$, and γ_n are the eigenvalues obeying the equality $\tan(\gamma) = \gamma$ (note that the first eigenvalue squared is γ_1^2 = 20.2). Since numerical values γ_n rapidly decrease when n increases, exponential terms decay and the parabolic profile forms after the time period of $t > \tau_R/20$. In the other words, relaxation time can be estimated from Fo > 1/20, where $\mathrm{Fo} = a_{l,eff}t/R^2$ is the Fourier number.

Eq. (18) also shows that transient derivative $\partial T/\partial t$ no longer depends on r. Averaging Eq. (10) over the sphere volume (R is assumed to be constant here) yields ODE for the volume averaged temperature (15):

$$c_l m\frac{d\bar{T}}{dt} = -4\pi R^2 q_s. \tag{19}$$

For q_s = const, solution to Eq. (19) is

$$\bar{T} = T_0 - 3\frac{q_s R}{\lambda_{l,eff}}\frac{a_{l,eff}}{R^2}t. \tag{20}$$

Therefore, after decay of the exponential terms, Eq. (18) takes the form:

$$T(r,t) = \bar{T}(t) + \frac{3}{10}\frac{q_s R}{\lambda_{l,eff}}\left(1 - \frac{5}{3}\left(\frac{r}{R}\right)^2\right), \tag{21}$$

where the dependence of the temperature on time is absorbed in $\bar{T}(t)$ according to Eq. (20). Clearly, Eq. (21) coincides with Eq. (17), if $c_0 = \bar{T} + 3q_s R/10\lambda_{l,eff}$ and $c_2 = -q_s R/2\lambda_{l,eff}$.

Relations for c_0 and c_2 in Eq. (17) could also be obtained with no recourse to the analytical solution. Indeed, applying boundary condition (12) yields equality $c_2 = -q_s R/2\lambda_{l,eff}$, and substitution of Eq. (17) in Eq. (15) gives $\bar{T} = c_0 + (3/5)c_2$. According to Eq. (17), surface temperature is $T_s = c_0 + c_2$, and center temperature is $T_c = c_0$. Combining these relations gives:

$$T_s = \bar{T} - \frac{1}{5}\frac{Rq_s}{\lambda_{l,eff}},\ T_c = \frac{5}{2}\bar{T} - \frac{3}{2}T_s. \tag{22}$$

Substituting Eq. (4) in the first relation in Eq. (22), surface temperature can be related to the volume averaged and equilibrium temperatures, $\bar{T}$ and T_{eq}:

$$T_s = \frac{\tau_{eq}\bar{T} + \tau_l T_{eq}}{\tau_{eq} + \tau_l}, \tag{23}$$

where

$$\tau_l = \tau_R/15 \tag{24}$$

is the characteristic time scale of internal temperature relaxation to a quasi-steady (not necessary uniform) field. Note that the time instant $t = \tau_l$ corresponds to the Fourier number Fo = t/τ_R = 1/15, which is close to 1/20 obtained from the analytical solution. In the limit of $\tau_l/\tau_{eq} \ll 1$ temperature distribution becomes uniform, ($T_c - T_s \approx 0$, $T_s \approx \bar{T}$), while in the opposite limit of $\tau_l/\tau_{eq} \gg 1$ maximum gradient exists ($T_c - T_s \approx 5\left(\bar{T} - T_{eq}\right)/2$, $T_s \approx T_{eq}$). Note that the internal temperature gradient decays as $\bar{T} \to T_{eq}$. Thus, numerical value of ratio τ_l/τ_{eq} determines the magnitude of the internal temperature gradient in the droplet.

Using Eqs (4) and (23), heat balance equation, Eq. (14) can be written as

$$\frac{1}{1+\tau_l\left(\dot{m}/m\right)}\frac{d\bar{T}}{dt} = -\frac{\bar{T} - T_{eq}}{\tau_l + \tau_{eq}}. \tag{25}$$

Heat balance equation, Eq. (25), shows that the time scale of volume-averaged temperature relaxation to its equilibrium value, T_{eq}, is determined by

$$\tau_{eq}^* = \tau_l + \tau_{eq}. \tag{26}$$

According to Eqs (22) to (25), the difference between T_c, T_s and $\bar{T}$ decays during the time period proportional to τ_{eq}^*. Thus, the value of τ_{eq}^* given by Eq. (26) is also a time scale characteristic of the temperature equalization inside the droplet.

Solving Eq. (25) and using Eq. (23), surface temperature of the droplet is obtained. Applicability of this approach has important limitations. First, at small times surface and center temperatures instantly become different even though initially $T_c = T_s$. Indeed, Eq. (23) shows that the surface temperature at small times is $T_s \xrightarrow[t\to 0]{} T_0 + \left(T_{eq} - T_0\right)\left(\tau_l/\tau_{eq}\right)\Big/\left(1+\left(\tau_l/\tau_{eq}\right)\right)$, instead of $T_s \xrightarrow[t\to 0]{} T_0$. This clearly demonstrates that parabolic approximation is invalid, since at $t \ll \tau_l$ the quasi-steady parabolic profile does not yet exists. To relax this controversy, it has been suggested by Dombrovsky and Sazhin [2003] to artificially smooth the transient dependence $T_s(t)$ at small times by applying the following *ad hoc* relation:

$$\frac{T_s - \bar{T}}{T_{eq} - \bar{T}}\frac{1+\left(\tau_l/\tau_{eq}\right)}{\left(\tau_l/\tau_{eq}\right)} = 1 - \exp\left(-100\sqrt{5\left(\tau_l/\tau_{eq}\right)}\frac{t}{15\tau_l}\right). \tag{27}$$

It can be seen that Eq. (27) converts to Eq. (23) as $t/\tau_l \to 0$.

Another limitation of this approach stems from the assumption that the temperature profile is monotone, which may not be true if the droplet moves through the zones with significantly different ambient temperatures.

Polynomial approximation. The above limitations of the parabolic approximation can be overcome by using higher order polynomials (cf. Eq. (17)):

$$T(r) = c_0 + c_2\left(r/R\right)^2 + c_p\left(r/R\right)^p, \tag{28}$$

where $p > 2$. This approach with $p = 4$ has been successfully used by Subramanian et al. [2005] for modelling lithium intercalation in the particles of active materials in lithium-ion batteries. Note that both in droplet evaporation and lithium intercalation the sought quantity is not the entire field in the sphere, but the surface value of temperature or lithium concentration. While applying this approach for droplet evaporation, we generalize its formulation to arbitrary polynomial power, p, and take into account the dependence of droplet radius on time.

Surface temperature, volume-averaged temperature and their difference can be obtained from Eq. (28):

$$T_s = c_0 + c_2 + c_p, \tag{29}$$

$$\bar{T} = \frac{3}{R^3}\int_0^R T(r) r^2 dr = c_0 + \frac{3}{5}c_2 + \frac{3}{p+3}c_p, \tag{30}$$

$$T_s - \bar{T} = \frac{2}{5}c_2 + \frac{p}{p+3}c_p. \tag{31}$$

Additionally, volume-averaged heat flux is determined as:

$$\bar{q} = \frac{3}{R^3}\int_0^R \left(-\lambda_{l,eff}\frac{\partial T}{\partial r}\right) r^2 dr = -\frac{\lambda_{l,eff}}{R}\left(\frac{3}{2}c_2 + \frac{3p}{p+2}c_4\right). \tag{32}$$

Substituting Eq. (28) to boundary condition (Eq. (12)) yields:

$$q_s = -\frac{\lambda_{l,eff}}{R}\left(2c_2 + pc_p\right). \tag{33}$$

Solving Eqs (32) and (33) results in:

$$c_2 = \frac{R}{\lambda_{l,eff}}\frac{2}{p-2}\left(q_s - \frac{p+2}{3}\bar{q}\right),\ c_p = \frac{R}{\lambda_{l,eff}}\frac{p+2}{p(p-2)}\left(-q_s + \frac{4}{3}\bar{q}\right). \tag{34}$$

In special case of parabolic profile $c_p = 0$, $\bar{q} = 3q_s/4$ and $c_2 = -Rq_s/2\lambda_{l,eff}$, which is consistent with the previous section of this paper. To use Eqs (34), the volume-averaged heat flux, $\bar{q}$, must be obtained. This is done by averaging gradients of the left and right hand sides of Eq. (10):

$$\frac{3}{R^3}\int_0^{R(t)} \frac{\partial}{\partial r}\left(c_l\rho_l\frac{\partial T}{\partial t}\right) r^2 dr = \frac{3}{R^3}\int_0^{R(t)} \frac{\partial}{\partial r}\left(\frac{1}{r^2}\frac{\partial}{\partial r} r^2 \lambda_{l,eff}\frac{\partial T}{\partial r}\right) r^2 dr \tag{35}$$

Performing integration in Eq. (35) using Eq. (34), the following ODE is obtained for the volume-averaged heat flux:

$$\frac{d\bar{q}}{dt} = -\frac{1}{\tau_R}\frac{4(p+1)(p+2)}{p}\left(\bar{q} - \frac{3}{4}q_s\right) - \frac{\dot{m}}{m}\left(\bar{q} - q_s\right). \tag{36}$$

Initial condition for Eq. (36) is determined by the initial temperature distribution. For uniform initial temperature field the initial condition for Eq. (36) is $\bar{q}(0) = 0$. If $\dot{m} = 0$, then asymptotic steady volume-averaged heat flux is $\bar{q} = 3q_s/4$. When this value is achieved, the parabolic profile forms, for which $c_p = 0$ and Eq. (17) holds.

Using Eqs (31) and (34), difference between surface temperature and volume-averaged temperature is obtained:

$$T_s - \bar{T} = \frac{2}{5}c_2 + \frac{4}{7}c_p = -\frac{1}{5}\frac{Rq_s}{\lambda_{l,eff}}\phi_p, \tag{37}$$

where

$$\phi_p = \frac{1}{p+3} + \frac{4}{3}\frac{p+2}{p+3}\frac{\bar{q}}{q_s}. \tag{38}$$

It can be shown that $0 \le \bar{q} < 3q_s/4$ and $\phi_p \le 1$. In special case of $p = 2$ volume-averaged heat flux is $\bar{q} = 3q_s/4$ and $\phi_p = 1$, which is consistent with Eq. (22). Using $4\pi R^2 q_s = c_l m\left(T_s - T_{eq}\right)/\tau_{eq}$, Eq. (37) can be written as

$$T_s = \frac{\tau_{eq}\bar{T} + \phi_p \tau_l T_{eq}}{\tau_{eq} + \phi_p \tau_l}, \tag{39}$$

which differs from its counterpart, Eq. (23), by the factor of ϕ_p. The corresponding heat balance equation, Eq. (25), takes the form

$$\frac{1}{1+\phi_p\tau_l\left(\dot{m}/m\right)}\frac{d\bar{T}}{dt} = -\frac{\bar{T} - T_{eq}}{\phi_p\tau_l + \tau_{eq}}. \tag{40}$$

Thus, modelling droplet evaporation would require simultaneous solving two ODEs for the volume averaged temperature, Eq. (40), and heat flux, Eq. (36). Surface temperature is then evaluated using Eq. (37).

It can be demonstrated that use of higher order polynomial profile significantly increases accuracy of predicting surface temperature at small times. For illustrative purposes, consider heating of non-evaporating sphere by constant external heat flux: $\dot{m} = 0$, $q_s = -q_{s,0}$, $q_{s,0} > 0$. In this case Eq (14) is reduced to

$$\frac{\tau_R}{T_*}\frac{d\bar{T}}{dt} = 3,\ \bar{T}(0) = T_0, \tag{41}$$

where $T_* = Rq_{s,0}/\lambda_{l,eff}$. As follows from Eq. (41), volume-averaged temperature increases linearly with time:

$$\left(\bar{T} - T_0\right)/T_* = 3t/\tau_R. \tag{42}$$

Solving Eq. (36) with initial condition $\bar{q}(0) = 0$ yields:

$$\bar{q} = -\frac{3}{4}q_{s,0}\left(1 - \exp\left(-\frac{4(p+1)(p+2)}{p}\frac{t}{\tau_R}\right)\right). \tag{43}$$

Using Eqs (37), (42) and (43), the following dependence of surface temperature on time is obtained:

$$\frac{T_s - T_0}{T_*} = 3\frac{t}{\tau_R} + \frac{1}{5}\begin{cases} 1, & p = 2 \\ 1 - \dfrac{p+2}{p+3}\exp\left(-\dfrac{4(p+1)(p+2)}{p}\dfrac{t}{\tau_R}\right), & p > 2 \end{cases}. \tag{44}$$

Approximate solution, Eq. (44), can now be compared with exact analytical solution, which is obtained by setting $r = R$ in Eq. (18):

$$\frac{T_s - T_0}{T_*} = 3\frac{t}{\tau_R} + \frac{1}{5} - \sum_{n=1}^{\infty}\frac{2}{\gamma_n^2}\exp\left(-\gamma_n^2\frac{t}{\tau_R}\right). \tag{45}$$

Neglecting higher order terms results in approximate relation:

$$\frac{T_s - T_0}{T_*} \approx 3\frac{t}{\tau_R} + \frac{1}{5}\left(1 - 0.495\exp\left(-20.2\frac{t}{\tau_R}\right)\right), \tag{46}$$

which is similar to Eq. (44). Analytic expressions can also be obtained for the center temperature.

Comparison of transient surface and center temperatures obtained for p = 2, 3, 4, 5, 6, 7 and 8 with the exact analytical solution and with the volume-averaged temperature is given in Fig. 2. Note that the relative temperatures, which asymptotically approach constant values, are shown.

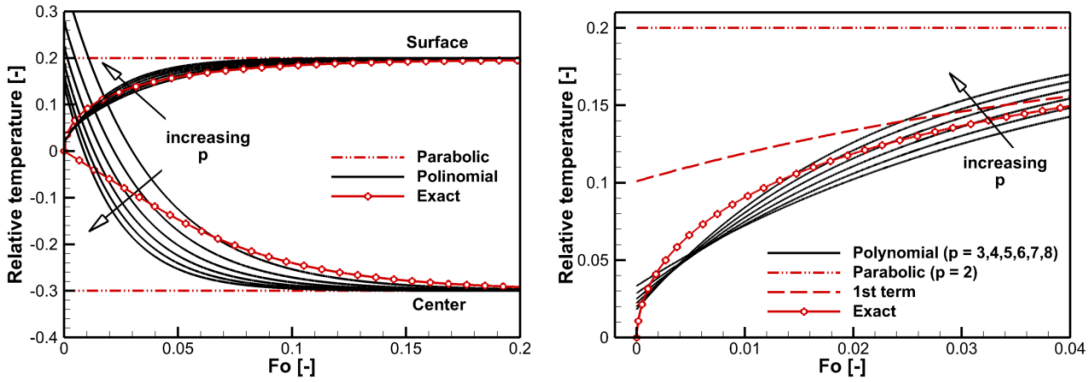

a) b)

Fig. 2. Simulated dependence of relative surface temperature $\left(T_s - \bar{T}\right)/T_*$ and center temperature $\left(T_c - \bar{T}\right)/T_*$ on time at constant surface heat flux: a) – $0 < \mathrm{Fo} < 0.2$, b) – $0 < \mathrm{Fo} < 0.04$ (surface temperature only)

It can be seen that at small times, $t < \tau_R/10$, surface temperature obtained for the parabolic profile (p = 2, horizontal lines in Fig. 2) differs significantly from the exact solution. At the same time, use of higher order polynomials results in much better agreement with it. Indeed, surface temperature at the very beginning of heating is

$$\frac{T_s - T_0}{T_*} = \frac{1}{5}\begin{cases} 1, & p = 2 \\ 1/(p+3), & p > 2 \\ 0, & \text{exact solution} \end{cases}, \tag{47}$$

which indicates, for example, that use of the fourth order polynomial reduces initial error by a factor of 7, compared to the parabolic approximation. Consideration of simulation results shown in Fig. 2 leads to the conclusion that optimum value of p lies in the range of 3 to 4 (p = 4 is used hereafter in this work). Note that the center temperature cannot be adequately predicted by the quasi-steady polynomial profile at small times. However, for the problem considered in this work, this is not crucial, since only surface temperature is required.

The advantage of the polynomial approximation is determined by the exponential relaxation of the volume-averaged heat flux in time (see Eq. (43)), with the relaxation time proportional to τ_R (in case of parabolic profile, such a relaxation is instantaneous). This advantage is particularly pronounced when the droplet is exposed to a rapidly changing external heat flux. As an example, consider two periodic functions $q_s(t)$. The first one is the stepping function defined as $q_s = -2q_{s,0}$ for $(k-1)T/2 < t < kT/2$ and $q_s = 0$ otherwise (k = 1, 2, …). The second one is a smooth function,

$q_s = -2q_{s,0}\sin^2(2\pi t/T)$. In both cases, time-averaged value of $q_s(t)$ is equal to $-q_{s,0}$. Time period T is chosen to set the Fourier number, $\mathrm{Fo}_T = T/\tau_R$, equal to 1/30.

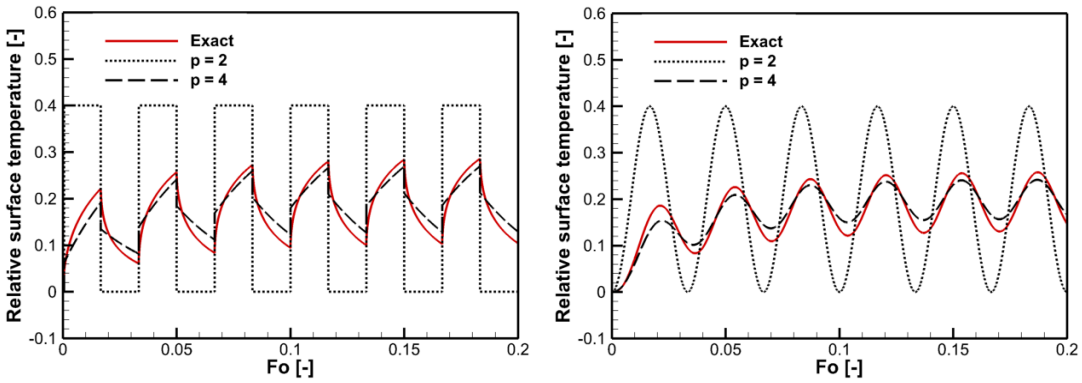

Fig. 3. Simulated dependence of relative surface temperature $(T_s - \bar{T})/T_*$ on time at periodic surface heat flux: a) stepwise, b) – smooth

It is clearly demonstrated in Fig. 3 that use of fourth order polynomial approximation replicates exact solution for the surface temperature with the high accuracy. This is a remarkable improvement compared to the performance of parabolic approximation, which results in an unacceptable error. It is noticed in the previous section, that the above error can also be reduced by the smoothing formulae, Eq. (27). However, this procedure can only be applied in case of monotone heating. On the contrary, polynomial approximation suggested in this work does not require artificial smoothing and it can be applied for arbitrary dependence of the external heat flux on time.

The heat balance integral method. Intrinsic limitation of the parabolic and polynomial approximations stems from the assumption that the temperature profile (either parabolic or higher order polynomial) is instantly established. As a result, in case of parabolic profile, both surface and internal temperatures are predicted incorrectly at small times. In case of higher order polynomial approximation, only surface temperature is predicted adequately, while the internal temperature is inadequate at small times. Both highly accurate surface temperature and qualitatively correct solution in the entire droplet interior can be obtained if the unsteady thermal boundary layer is considered near the droplet surface. The boundary of the thermal layer propagates with time towards the droplet center at a finite speed, obeying the overall heat balance in the droplet. This is the idea of classical method of heat balance integral by Goodman [1958]. Despite of the extensive literature reflecting application of this method, the authors are not aware of the works in which this method was applied to model droplet evaporation. Meanwhile, this method is an excellent candidate for being used in CFD spray modelling.

Consider the thermal layer having thickness of $\delta(t)$. Inside this layer temperature is approximated by the parabolic profile, and the initial temperature is set outside the layer:

$$T(r) = \begin{cases} c_0 + c_2\left((r-(R-\delta))/R\right)^2 & , \quad R-\delta \le r \le R \\ T_0 & , \quad 0 \le r \le R-\delta \end{cases}. \tag{48}$$

The boundary layer thickness varies in the range of $0 < \delta \le R$. The parabolic profile, Eq. (17), coincides with (48), when $\delta = R$. According to Eq. (48), volume-averaged temperature and surface temperature are calculated as

$$\bar{T} = T_0\left(1-\delta/R\right)^3 + c_0\left(1-\left(1-\delta/R\right)^3\right) + c_2\left(\delta/R\right)^3\left(1-\left(\delta/R\right)/2+\left(\delta/R\right)^2/10\right), \tag{49}$$

$$T_s = c_0 + c_2 \left(\delta / R\right)^2 . \tag{50}$$

Substituting Eq. (48) to boundary condition (12) yields $q_s = -2c_2 \left(\lambda_{l,eff} / R\right)\left(\delta / R\right)$ and

$$c_2 = -\frac{1}{2}\frac{q_s R}{\lambda_{l,eff}}\frac{R}{\delta}. \tag{51}$$

It follows from Eq. (48) that $c_0 = T_0$ if $\delta < R$. In this case, it can be obtained from Eqs (51) and (49):

$$\bar{T} = T_0 - \frac{1}{2}\frac{q_s R}{\lambda}\left(\frac{\delta}{R}\right)^2\left(1 - \frac{1}{2}\frac{\delta}{R} + \frac{1}{10}\left(\frac{\delta}{R}\right)^2\right). \tag{52}$$

Once the volume-averaged temperature is found from the heat balance equation, Eq. (14), relation (52) can be used to calculate the thickness of the thermal layer, δ. For a given thickness surface temperature is obtained from Eqs (50) and (51):

$$T_s = T_0 - \frac{1}{2}\frac{q_s \delta}{\lambda_{l,eff}}. \tag{53}$$

When the thickness of thermal layer expands to $\delta = R$, Eqs. (49), (52) and (50) yield:

$$c_0 = \bar{T} - \frac{3}{5}c_2,\ \bar{T} = T_0 - \frac{3}{10}\frac{q_s R}{\lambda_{l,eff}},\ T_s = \bar{T} - \frac{1}{5}\frac{q_s R}{\lambda_{l,eff}}, \tag{54}$$

which implies formation of the parabolic profile, Eq. (21). Therefore, surface temperature is evaluated as follows:

$$T_s = T_0 - \frac{1}{2}\frac{q_s \delta}{\lambda_{l,eff}},\ \text{if } \delta < R \text{ and } T_s = \bar{T} - \frac{1}{5}\frac{q_s R}{\lambda_{l,eff}},\ \text{if } \delta = R. \tag{55}$$

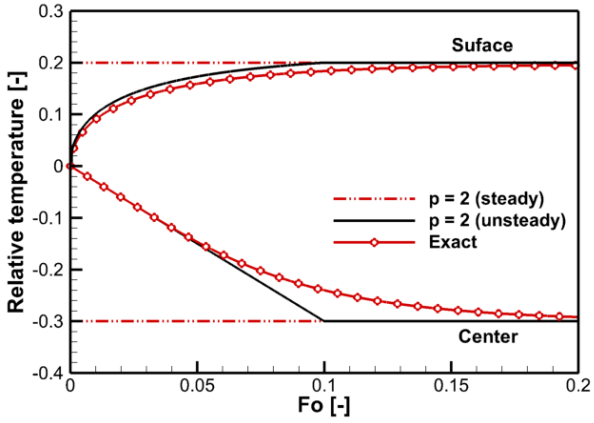

Fig. 4. Dependence of relative surface temperature $\left(T_s - \bar{T}\right)/T_*$ and center temperature $\left(T_c - \bar{T}\right)/T_*$ on time. Simulation by the heat balance integral method

For the temperature of droplet center it can be obtained

$$T_c = c_0 = \begin{cases} T_0, & \text{if } \delta < R; \\ \bar{T}(t) + \dfrac{3}{10}\dfrac{q_s R}{\lambda_{l,eff}}, & \text{if } \delta = R. \end{cases} \tag{56}$$

If $\dot{R}=0$ and q_s = const, then the thermal layer expands to the thickness of $\delta = R$ at the time instant of $t=\tau_R/10$; this corresponds to the Fourier number $\mathrm{Fo}=1/10$.

Comparison of the exact and approximate surface and center temperatures is shown in Fig. 4. It can be seen that even parabolic approximation of the temperature profile inside the thermal layer results in a very good agreement for both surface and center temperatures at all times. Maximum disagreement occurs at time interval around $\tau_R/10$, when transition to the quasi-steady parabolic profile occurs.

STIFFNESS OF THE DROPLET HEAT BALANCE EQUATION: NUMERICAL TREATMENT

Accuracy of droplet heating and evaporation simulations is mainly determined by solving the heat balance equation, Eq. (14), which can be formulated as

$$\frac{d\bar{T}}{dt} = -\frac{T_s - T_{eq}}{\tau_{eq}} - \frac{\dot{m}}{m}\left(\bar{T} - T_s\right),\ \bar{T}\left(t^n\right) = \bar{T}^n \tag{57}$$

for every droplet. Eq. (57) is solved jointly with the droplet mass balance equation and is complemented by the internal heat transfer model which provides coupling between T_s and $\bar{T}$. Such a system is characterised by three distinct time scales, τ_l, τ_{eq} and τ_{evap}, the latter being droplet evaporation time: $\tau_{evap} = \rho_l d_0^2 \Big/ \left(4\mathrm{Nu}^* \left(\lambda_g / c_{p,vap}\right) \ln\left(1 + B_T\left(T_{wb}\right)\right)\right)$.

Bearing in mind wide range of droplet sizes and, therefore, associated time scales, the key requirement to the numerical methodology is its absolute stability regardless of the time step and droplet thermal inertia. Such a methodology must also ensure that droplet temperature lies within the certain bounds, *i.e.* between initial and equilibrium temperature. Both requirements are satisfied by the implicit schemes. Let the equilibrium temperature (which is equal to the wet bulb temperature in the absence of radiation) is known for the given ambient temperature. Fully implicit first order scheme is formulated as follows:

$$\frac{\bar{T}^{n+1,i+1} - \bar{T}^n}{\Delta t} = -rhs\,\frac{\bar{T}^{n+1,i+1} - T_{eq}}{\bar{T}^{n+1,i} - T_{eq}}, \tag{58}$$

where

$$rhs = \frac{T_s - T_{eq}}{\tau_{eq}} + \frac{\dot{m}}{m}\left(\bar{T} - T_s\right), \tag{59}$$

is the right hand side of Eq. (57) evaluated at time instant $t = t^n$, and i is the iteration number such as $\bar{T}^{n+1,0} = \bar{T}^n$. Right hand sides of Eqs (58) and (57) coincide when iterations converge. It follows from Eq. (58) that

$$\bar{T}^{n+1,i+1} = \left(\bar{T}^n + rhs\,\frac{T_{eq}}{\bar{T}^{n+1,i} - T_{eq}}\Delta t\right) \Bigg/ \left(1 + rhs\,\frac{1}{\bar{T}^{n+1,i} - T_{eq}}\Delta t\right). \tag{60}$$

Setting $\left(\bar{T}^{n+1,i+1} - \bar{T}^n\right)/\Delta t \approx dT/dt$, it can also be found

$$\bar{T}^{n+1,i+1} = T_{eq} + \left(\bar{T}^{n+1,i} - T_{eq}\right)\exp\left(-\frac{rhs}{\bar{T}^{n+1,i} - T_{eq}}\Delta t\right). \tag{61}$$

Both in (60) and (61), we assume that *rhs* and T_{eq} are frozen during the time step, Δt. Numerical tests have shown that Eqs (60) and (61) yield very close results when the time step is small enough, and Eq. (61) is therefore recommended to avoid computations of the exponential function.

To solve Eq. (57), it is not necessary to resolve thermal relaxation time inside the droplet, τ_l, even if $\tau_l < \tau_{eq}$. Note that the advantage of an accurate determination of the droplet surface temperature manifests itself when $\tau_l > \tau_{eq}$. Thus, to accurately resolve all the time scales intrinsic to the problem considered, the time step should be chosen as $\Delta t < \min\left(\tau_{eq}, \tau_{evap}\right)$. When the heat balance equation is solved jointly with the droplet momentum equation, the above constraint is further refined as

$$\Delta t < \min\left(\tau_{eq}, \tau_{velo}, \tau_{evap}\right), \tag{62}$$

where τ_{velo} is the droplet velocity relaxation time scale. Order of magnitude analysis shows that typically $\tau_{eq} = \mathrm{O}\left(\tau_{velo}\right)$ and $\tau_{eq} << \tau_{evap}$, which makes the problem stiff. Indeed, droplet temperature changes rapidly from its initial value of T_0 to the equilibrium one, T_{eq}, during short initial transient period of order of τ_{eq}. The initial transient period is then followed by the relatively long quasi-steady period (of order of τ_{evap}) when the temperature is close to T_{eq}. As a result, the time step obeying inequality (62) is unreasonably and, in case of very large amount of droplets, unacceptably small during the most of the droplet life time.

In fact, condition (62) must only be satisfied during the initial transient period which expires as soon as droplet temperature gets close to T_{eq}. At a later time, the time step should resolve much larger time scale, τ_{evap}. These considerations dictate the following choice of the time step:

$$\frac{1}{\Delta t} = \frac{1}{C}\left(\frac{\delta}{\min\left(\tau_{eq}, \tau_{velo}\right)} + \frac{1-\delta}{\tau_{evap}}\right), \tag{63}$$

where $C < 1$; values of τ_{eq} and τ_{velo} are evaluated at the initial temperature, while τ_{evap} is evaluated at T_{eq}. Parameter $\delta = \left|\overline{T} - T_{eq}\right| / \left|T_0 - T_{eq}\right|$ changes from 1 down to 0 and it reflects the completeness of temperature relaxation to its asymptotic (equilibrium) limit. Since $\tau_{eq} = \mathrm{O}\left(\tau_{velo}\right)$, the value of δ also shows the degree of velocity relaxation. At the beginning of the initial transient period of droplet heating or cooling, $\delta \approx 1$ and $\Delta t \approx C\tau_{eq}$, while after the equilibrium temperature is achieved $\delta \to 0$ and $\Delta t \approx C\tau_{evap}$. Due to such an adaptation of the time step, number of time steps required for a sufficiently accurate numerical solution is weakly sensitive to the ratio τ_{eq}/τ_{evap}, provided that the proportionality coefficient, C, is small enough.

To illustrate the above conclusion, consider evaporation of water droplet with initial diameter of d_0 = 0.1 mm and initial temperature of T_0 = 20ºC. Ambient air temperature, T_{air}, is set constant. Thermal radiation is not present which implies $\tau_{eq} = \tau_{conv}$ and $T_{eq} = T_{wb}$. For T_{air} = 20ºC it can be found that τ_{conv}/τ_{evap} = 0.0062, whilst for T_{air} = 1400ºC the above ratio is equal to 0.091. In both cases $\tau_{conv} << \tau_{evap}$. At low ambient temperature (say, 20ºC) the ratio τ_{conv}/τ_{evap} is much less than that at high ambient temperature (say, 1400ºC) which aggravates the stiffness of the problem.

Predicted droplet evaporation dynamics is shown in Fig. 5 to Fig. 7. Transient dependencies of droplet evaporation rate, dm/dt, are seen to be qualitatively different in cases of high and low ambient air temperatures (compare Fig. 5, a, and Fig. 6, a). This is due to the fact that in the first case (high ambient temperature) the wet bulb temperature is higher than the initial one, which is opposite to the second case of low ambient temperature. Dependence of droplet evaporation rate on time is non-monotone in Fig. 5 (high ambient temperature): it increases initially because of rising droplet temperature and decreases afterwards because of decreasing droplet surface area. Alternatively, in Fig. 6 (low ambient temperature) droplet evaporation rate decreases during the entire droplet life time.

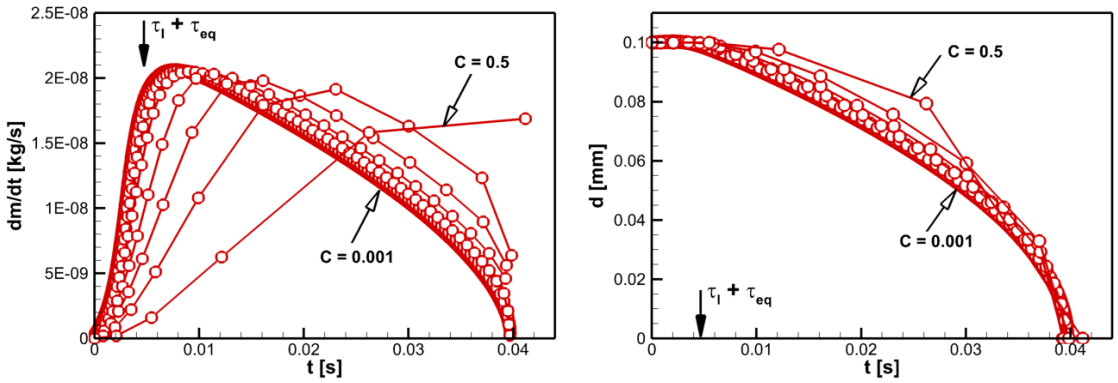

a) b)

Fig. 5. Sensitivity of the numerical solution to the time step coefficient, C, (high ambient temperature): a) – droplet evaporation rate; b) – droplet diameter. Lines for C = 0.001, 0.002, 0.005, 0.01, 0.02, 0.05, 0.1, 0.2 and 0.5 are shown. Water, d_0 = 0.1 mm, V_0 = 10 m/s, T_0 = 20ºC, T_{air} = 1400ºC

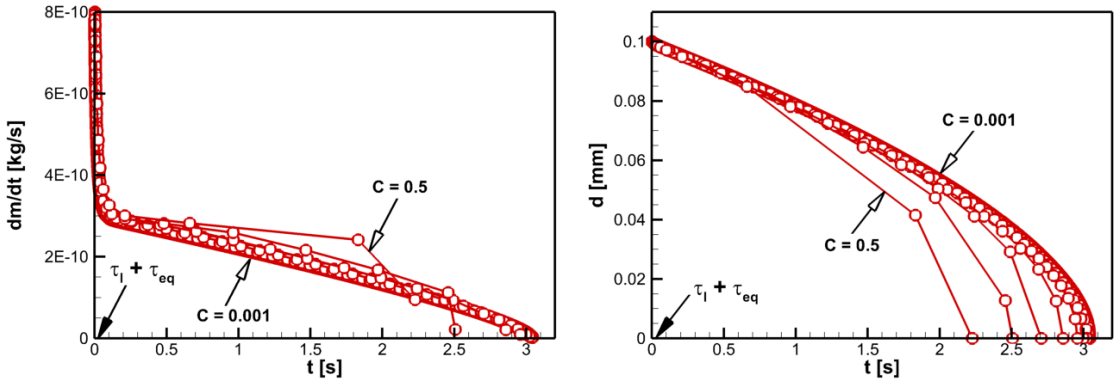

a) b)

Fig. 6. Sensitivity of the numerical solution to the time step coefficient, C, (low ambient temperature): a) – droplet evaporation rate; b) – droplet diameter. Lines for C = 0.001, 0.002, 0.005, 0.01, 0.02, 0.05, 0.1, 0.2 and 0.5 are shown. Water, d_0 = 0,1 mm, V_0 = 10 m/s, T_0 = 20ºC, T_{air} = 20ºC

When the ambient temperature is low, only a minor fraction of droplet mass is vaporized during the initial transient period, when all the parameters change rapidly (see Fig. 6 and Fig. 7, b). As a result, even poor resolution of the initial transient period (C > 0.2) still makes it possible to obtain qualitatively correct solution, and the error in predicting droplet life time does not exceed 20-30%. At high ambient temperatures, quality of the numerical solution deteriorates severely if C > 0.2 when predicted droplet evaporation rate is qualitatively incorrect (see Fig. 5 and Fig. 7, a). Despite of that, droplet life time is still predicted at a surprisingly good accuracy. In all the cases, simulation results (Fig. 5 to Fig. 7) show that reasonable accuracy can be obtained if C < 0.1, and the solution is practically insensitive to the time step if C < 0.05.

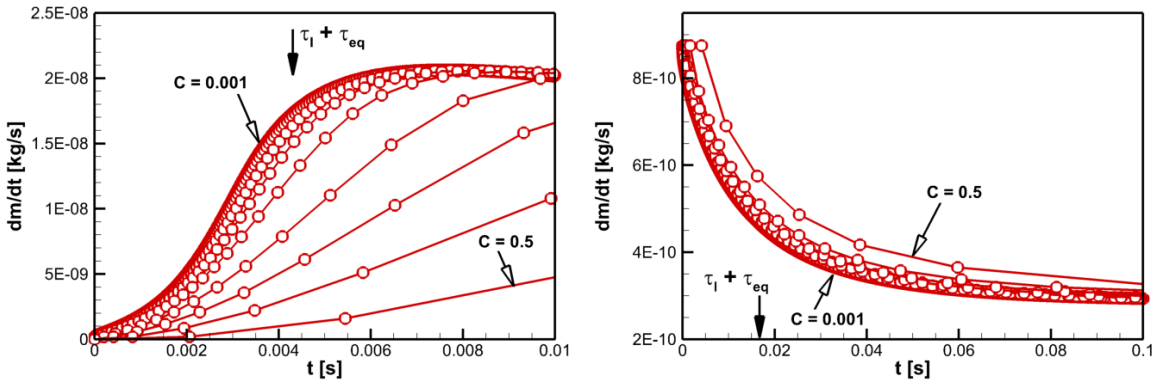

a) b)

Fig. 7. Sensitivity of the numerical solution to the time step coefficient, C, (initial transient period): a) – high ambient temperature, T_{air} = 1400ºC; b) – low ambient temperature, T_{air} = 20ºC. Lines for C = 0.001, 0.002, 0.005, 0.01, 0.02, 0.05, 0.1, 0.2 and 0.5 are shown. Water, d_0 = 0,1 mm, V_0 = 10 m/s, T_0 = 20ºC

HEATING AND EVAPORATION OF AN ISOLATED DROPLET

Droplet heating and evaporation model developed in this work has been extensively validated by Snegirev *et al.* [2011] against published and authors' experimental data for two liquids (water and acetone) of considerably different volatility. In this section the performance of simplified methods, in which internal temperature gradient is approximately taken into account, is demonstrated.

Basic option is numerical or analytical solution of heat conductivity equation, Eq. (16). In this work, we use an implicit finite-volume scheme to discretize Eq. (16), and the linearized system of algebraic equations is then solved by TDMA algorithm at every time step. Numerical solution is checked to ensure grid and time step independence and thus obtained solution therefore regarded as "exact". Of three simplified approaches used in this work, the parabolic and polynomial profiles are referred as "steady" (being in fact quasi-steady, its evolvement in time is accounted for by the time-dependent polynomial coefficients), and the integral heat balance method is called "unsteady" due to transient development of thermal boundary layer. Potentially, higher order polynomial could also be used inside the boundary layer; for the purpose of this work, parabolic profile is found to be sufficient.

To illustrate performance of all the above approaches, the experimental conditions by Maqua *et al.* [2008] have been replicated in the simulations. In these experiments, monodisperse droplets travel along straight trajectories at a controlled distance between the droplets. To allow for the effect of droplets on the velocity and temperature fields in the ambient gas by adjusting values of Nusselt and Sherwood numbers, an *ad-hoc* coefficient is introduced to. In the simulations we used the same coefficient as Maqua *et al.* [2008]. We also used the dependence of droplet velocity on time measured in the same experiment. It is claimed in the cited paper that experimental methodology measures volume-averaged droplet temperature. Measurement results are compared with the predictions in Fig. 8 which further supports above conclusions on applicability of steady (parabolic, and polynomial) and unsteady (heat balance integral) approximations.

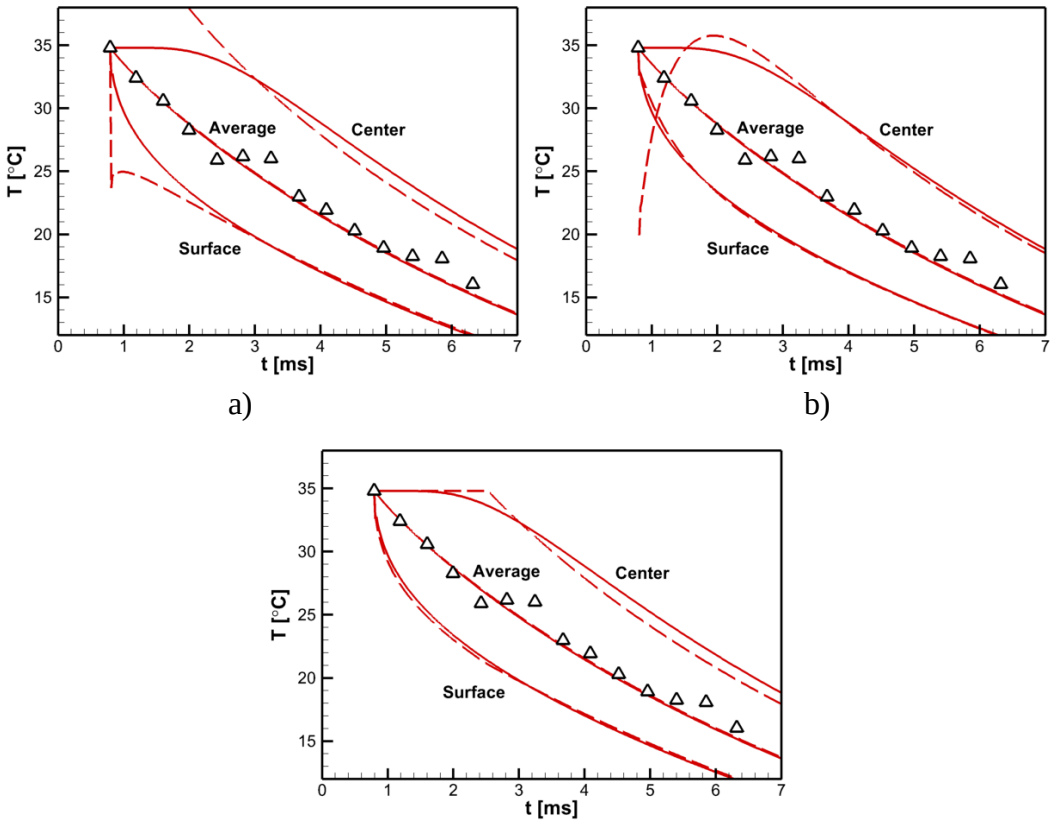

Fig. 8. Acetone droplet temperature during droplet evaporation in experimental conditions by Maqua *et al.* [2008]. d_0 = 0.143 mm, T_0 = 34.8°C, T_{air} = 21.5°C. Symbols – measurements Maqua *et al.* [2008], solid line – exact solution of heat conductivity equation, dashed lines: a) – parabolic approximation, b) – polynomial approximation, p = 4, c) – heat balance integral method, p = 2

Although at small times a considerable temperature gradient is predicted inside the droplet (Fig. 8), this gradient rapidly disappears during initial transient period when only small fraction of droplet mass is evaporated. As a result predicted droplet evaporation time appears to be practically the same regardless of whether this temperature gradient is considered or not. It can be shown that the effect of the internal temperature gradient is determined by the time scale ratio τ^*_{eq}/τ_{evap} which increases with the ambient temperature being greater for more volatile liquids (see Snegirev *et al.* [2012]).

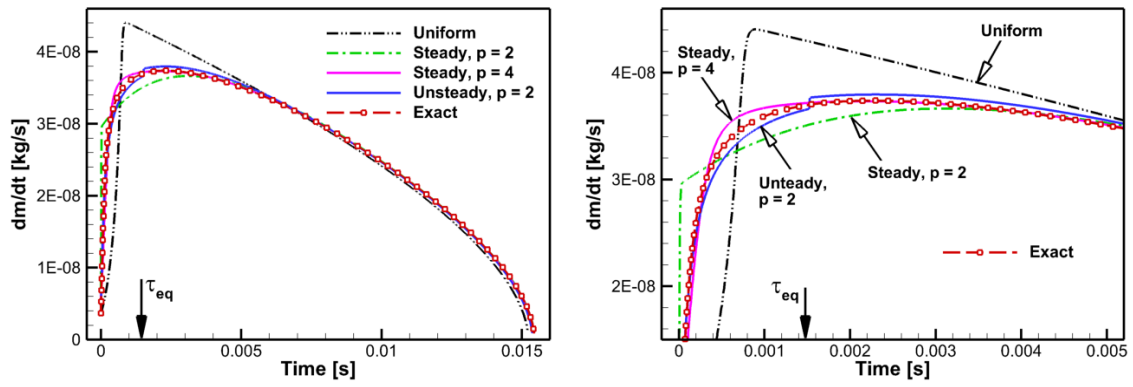

Fig. 9. Predicted acetone droplet evaporation rate (d_0 = 0.1 mm, T_{air} = 1400°C, initial droplet velocity V_0 = 10 m/s, droplet decelerates due to aerodynamic friction while travelling in stagnant air)

Performance of different approaches which take the internal temperature distribution into account is demonstrated in Fig. 9. It can be seen in Fig. 9 that neglecting internal temperature gradient results in a significant error in predicted evaporation rates at the initial stages of droplet evaporation (in this case $\tau_{eq}^{*}/\tau_{evap} \approx 0.1$). Use of any of the approximate methods described in this work produces reasonable agreement with the exact solution, although, as expected, parabolic approximation exhibits highest deviation at small times. Excellent agreement occurs if either polynomial approximation or integral heat balance method is used. In all the cases, predicted droplet life time is practically the same.

MODELLING AND SIMULATIONS OF TURBULENT SPRAYS

To simulate the carrier gas flow, the in-house Fire3D code (for example, see Snegirev *et al.* [2010]) has been applied, which solves transient Navier-Stokes equations for multi-component gas flow (including that with non-premixed combustion). Either Favre-averaged (URANS version) or filtered (LES version) equations are discretised by means of the finite volume method, and structured non-uniform Cartesian meshes are used. Second-order symmetric differencing is used in the approximations of the diffusion terms. Upwind TVD and bounded CD schemes are employed to approximate convective terms in scalar and velocity equations respectively, keeping the order of approximation close to two wherever possible, and yet ensuring that monotonicity of the solution is preserved. Three-layer backward second-order accurate approximation is used for time advancement. Multigrid-accelerated pressure correction technique is applied to couple the pressure and velocity fields in the low Mach number limit and to satisfy the continuity equation.

In LES, the subgrid stress tensor is modelled through the static Smagorinsky approach, with the Smagorinsky constant of $C_S = 0.1$ is used after its successful application in modelling of turbulent reacting jets and buoyant plumes. In the vicinity of solid walls, the mixing length in the subgrid viscosity formula is made proportional to the distance to the nearest wall.

A particle tracking (Lagrangian) approach is applied to model the evaporating spray. Given the gas flow characteristics, multiple discrete droplets are tracked along their trajectories. To make computations feasible, the momentum (as well as mass and energy) conservation equation is considered for a group of similar droplets (parcels). The spray submodel in Fire3D includes the following components: droplet movement (drag and gravity forces, spherical drag law), droplet dispersion by turbulence (stochastic subgrid eddy life time model), droplet heating (with the internal temperature gradient taken into account), droplet evaporation (the Abramzon-Sirignano model), inter-phase exchange, nozzle performance and spray atomization. For the latter, instantaneous atomization is assumed with prescribed probability distributions for the initial droplet size (combined log-normal/Rosin-Rammler: log-normal for $d < d_{v50}$ and Rosin-Rammler otherwise, d_{v50} is the median volumetric diameter) and velocity magnitude (Gaussian with mean velocity magnitude V_0, rms is set $0.1V_0$). Each droplet trajectory is launched at a randomly chosen point at a nozzle cross-section, and initial droplet velocity vectors uniformly fill the cone of prescribed angle. In the simulations shown in this work, we did not take into account droplet collisions and secondary break-up.

For droplet heating and evaporation, three approaches described above are incorporated in the spray model. Recall, however, that both higher order polynomial and integral heat balance method perform better than the parabolic approximation at small times, $t < \tau_l$. If the droplet evaporates in a homogeneous media and its surface is exposed to heat flux monotonically varying in time, then use of the integral heat balance method is justified. This method, being computationally inexpensive, provides good accuracy at all times, not only for the surface temperature but also for the droplet interior even with $p = 2$. Alternatively, if the droplet travels in the environment with spatially

inhomogeneous temperature distribution and therefore exposed to rapidly and non-monotonically varying heat flux, then the polynomial approximation with p = 4 is recommended. By this method, surface temperature can be predicted with the sufficient accuracy at all times, while the internal temperature distribution can only be predicted after the relaxation time expires. Simulation results shown in this work were obtained with the polynomial approximation.

Prior to this work, Fire3D model and code was applied to simulate water sprays and its interaction with buoyant turbulent diffusion flames (fire suppression), both in URANS [Snegirev and Lipjainen, 2008] and LES [Snegirev *et al.,* 2010] modes conventionally assuming uniform droplet temperature. In this work, this model and code has been amended by taking the internal temperature gradient into account. It has been validated by simulating experimental conditions relevant not only to fire suppression but also to liquid fuel injection, dispersion and vaporization. Validation results are demonstrated below for water, acetone, and diesel fuel sprays.

Water spray. Experimental scenario by Yoon *et al.* [2004] is considered, in which unconfined fine water spray in stagnant air was investigated. Nozzle and spray parameters are as follows: nozzle diameter D = 2 mm, water flow rate 0.25 kg/s, initial droplet velocity V_0 = 80 m/s, initial liquid temperature and ambient air temperature $T_0 = T_{air}$ = 300 K. As stated by Yoon *et al.* [2007], numerical values of Weber and Ohnesorge numbers calculated for the liquid jet injected from the nozzle ($\mathrm{We} = \rho_l V_0^2 D/\sigma_l$ = 174·10^3, $\mathrm{Oh} = \mu_l/\sqrt{\rho_l D \sigma_l}$ = 0.0023) and Weber number corresponding ambient gas density $\mathrm{We}_g = \rho_g V_0^2 D/\sigma_l$ = 215 are all high enough to safely assume rapid liquid atomization immediately near the nozzle outlet. The latter conclusion justifies approximate approach used in this work to model liquid atomization. In the simulations, ambient air was assumed to be dry.

This series of simulations was undertaken to calibrate the model by adjusting parameters of the initial droplet size distribution (median volumetric diameter, d_{v50}, and spread parameter, γ) and spray cone angle, φ. Based on the droplet diameters measured downstream the nozzle outlet, initial median volumetric diameter (extrapolated to the nozzle outlet location) was estimated as d_{v50} = 0.102μ. Three cone angles 15º, 20º, and 30º were considered. The best agreement with the experimental observations of the near field spray shape was observed in simulations with φ = 20º (see Fig. 10). Predicted shape of starting and developed spray is demonstrated in Fig. 11, which shows that droplet temperature in the spray periphery is close to the wet bulb temperature in dry air, while near the spray axis it is much higher being close to the initial liquid temperature. This is the indication of low evaporation rate near the spray axis which is reduced due to high vapour concentration, being close to the saturation one. Consideration of Fig. 11 also shows that smaller droplets concentrate in the near-axial region being driven by the entrained air which flows radially from spray periphery to its axis; having greater inertia, large droplets dominate at spray periphery.

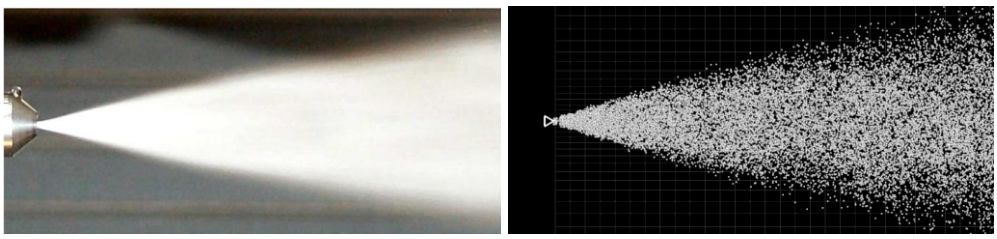

a) b)

Fig. 10. Near field of fine water spray: a) – experiment Yoon *et al.* [2004]; б) – instantaneous droplet locations. Fire3D model, d_{v50} = 0.102μ, γ = 2.25, φ = 20º

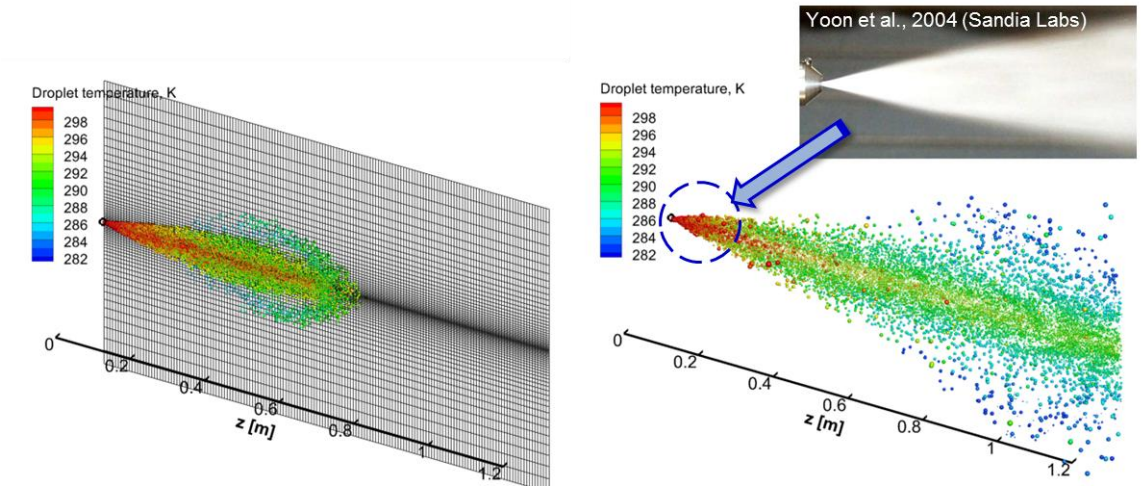

a) b)

Fig. 11. Simulation of fine water spray in experimental conditions by Yoon *et al.* [2004]: a) – computational mesh and instantaneous droplet locations in axial plane of the starting spray; b) – instantaneous droplet locations in axial plane of developed spray. Droplets are coloured by its temperature, size is proportional to the droplet diameter.
Fire3D model, $d_{v50} = 0.102\mu$, $\gamma = 2.25$, $\varphi = 20^{o}$

For $\varphi = 20^{o}$ and $d_{v50} = 0.102\mu$ sensitivity of the predictions to the spread parameter, γ, was examined by performing simulations with $\gamma = 1.5$, 2.25, and 3. Worth noticing that the shape of droplet size distribution is very different for these three values. In case of $\gamma = 1.5$ (this value was recommended by Yoon *et al.* [2004] and [2007]) significant amounts of small (with diameter less than d_{v50}) and large (diameter larger than d_{v50}) are present. Alternatively, size variation around d_{v50} is much less if $\gamma = 3$. Spray simulation results for three above values of γ are illustrated in Fig. 12 where predicted radial distributions of mean droplet diameter and axial droplet velocity at a certain distance from the nozzle outlet are compared to the measurements by Yoon *et al.* [2004]. It can be seen that the best (and reasonably good) representation of measured droplet diameters was achieved for $\gamma = 2.25$.

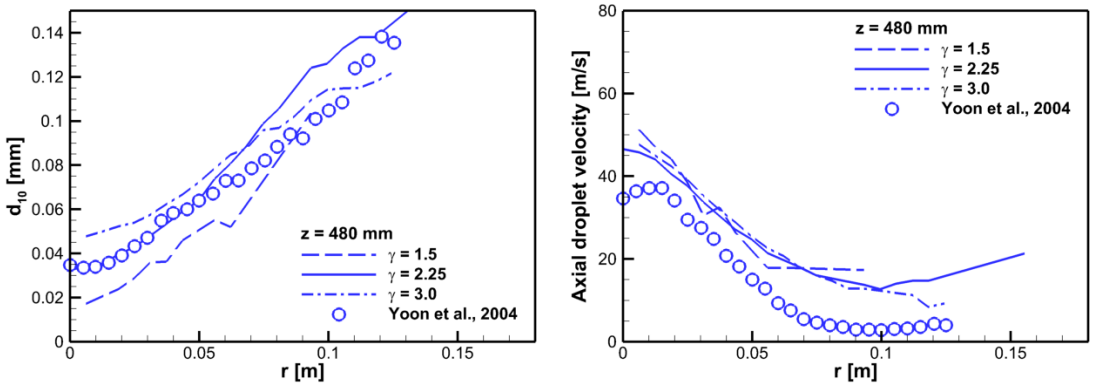

a) б)

Fig. 12. Radial distributions of mean droplet diameter (a) and axial droplet velocity (b) at a distance of 0.48 m from the nozzle outlet. Circles – measurements Yoon *et al.* [2004], lines – predictions by Fire3D model with different values of dispersion coefficient, γ, of the initial droplet size distribution

In the simulations performed so far droplet diameters and velocities at spray periphery were typically overestimated. A possible reason for this is that secondary break-up of large droplets was not activated in the model. Note, however, that in spray simulations Yoon *et al.* [2007] similar effect was observed although secondary break-up was taken into account. Also, Fig. 12 shows that droplet axial velocity is

overestimated by the predictions. Despite of the above shortcomings, it can be concluded that the spray model produced favorable quantitative agreement with the available measurements. This indicates that the effect of droplet collisions and secondary break-up occurring in the nozzle vicinity where both droplet concentration and velocity are high can be approximately taken into account by the appropriate choice of the initial droplet size distribution at the nozzle outlet location. Such an approach is justified in those applications where length of the dense part of the spray is much less than other length scales (*e.g.* distance from the sprinkler to the fire source in fire suppression scenarios).

Acetone spray. In this part of work, the spray model was applied to replicate the experimental conditions described by Chen et al. [2006]. Turbulent vapour-air jet flow with atomized acetone droplets is discharged through the cylindrical nozzle (9.8 mm diameter) in the air co-flow (3 m/s velocity). Similar to the experiments, the following range of parameters was considered in the simulations: jet Reynolds number 15800 to 31600, droplet SMD at nozzle outlet 13.7 to 23.9μ, liquid flow rate at nozzle outlet 7 to 11.7 g/min. Design of the nozzle used in the experiments by Chen et al. [2006] ensures complete liquid atomization at the nozzle outlet. Instantaneous simulated flow field for one of the sprays for which experimental data is available (jet Reynolds number 15800, droplet SMD at nozzle outlet 13.7μ, liquid flow rate at nozzle outlet 7 g/min) is illustrated in Fig. 14. To validate the model predictions, we used measured radial distributions of mean droplet velocity and liquid mass flow rate at different distances from the nozzle. Comparison shown in Fig. 14 demonstrates reasonable agreement particularly for velocity profiles although liquid mass flow rate appears to be underestimated.

Diesel fuel. To validate the spray model in diesel engine-like conditions, numerical simulation of starting diesel spray was undertaken. Unlike two above cases, starting spray is considered here, and propagation speed of the spray tip is examined. In the simulations, experimental conditions similar to those described by Sazhin *et al.* [2008] are replicated. In the experiments, sprays injected through a single-hole nozzle of 0.2 mm diameter into compressed air at temperature 540 K and pressure 2 and 6 MPa in a cylindrical chamber (50 mm diameter and 80 mm length). Note that for the liquid fuel considered, boiling temperature at 2 and 6 MPa is equal to 722 K and 831 K respectively. Spray penetration data were obtained by Sazhin *et al.* [2008] from the analysis of visible part of the spray in high-rate video recordings (up to 4500 frames per second), combined with the measurements of liquid injection rate. Liquid volume of 30 mm^3 was injected during 2 ms at a rate shown in Fig. 15 (a) by the solid line. In the simulations, oscillating experimental curve was approximated by the experimental fit also shown in Fig. 15 (a). The instantaneous atomization model used in this work implies that prescribed droplet size distribution is extrapolated to the nozzle outlet location. For the combined log-normal and Rosin-Rammler distribution used in the simulations we assumed $d_{v50} = 8\mu$ (this is in accord with the data by Sazhin *et al.* [2008]) and $\gamma = 2.25$. Cone angle was taken 15°, and initial droplet temperature was set 400 K. Nozzle outlet was located at the center of the chamber plane side, and the spray was injected vertically along the chamber axis. Vapour composition was represented by the molecule $C_{15}H_{26}$. Thermal and transport properties were taken from Sazhin *et al.* [2005] and a number of sources cited therein.

Predicted instantaneous droplet locations in a propagating spray are visualized in Fig. 16. Since the vapour is transparent, it is reasonable to expect that the experimentally recorded spray length corresponds to the region with droplet concentration higher than a particular threshold. At the initial stage of spray development its visible length grows, and the spray tip also coincides with the front edge of vapour cloud. Since all the axial gradients are high at the spray edge, its location is well defined at this stage.

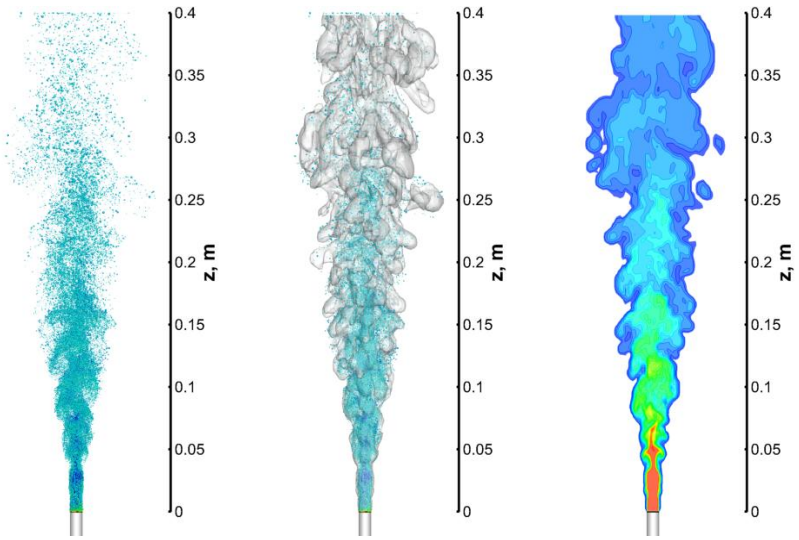

a) b) c)

Fig. 13. Instantaneous resolved flow field in the acetone spray (low speed, fine droplet spray LFS by Chen *et al.* [2006]): a) – droplet locations, coloured by liquid temperature; b) – iso-surface of vapour mole fraction 0.2%; c) – vapour mole fraction in the axial plane. Fire3D model, mesh 64x64x200

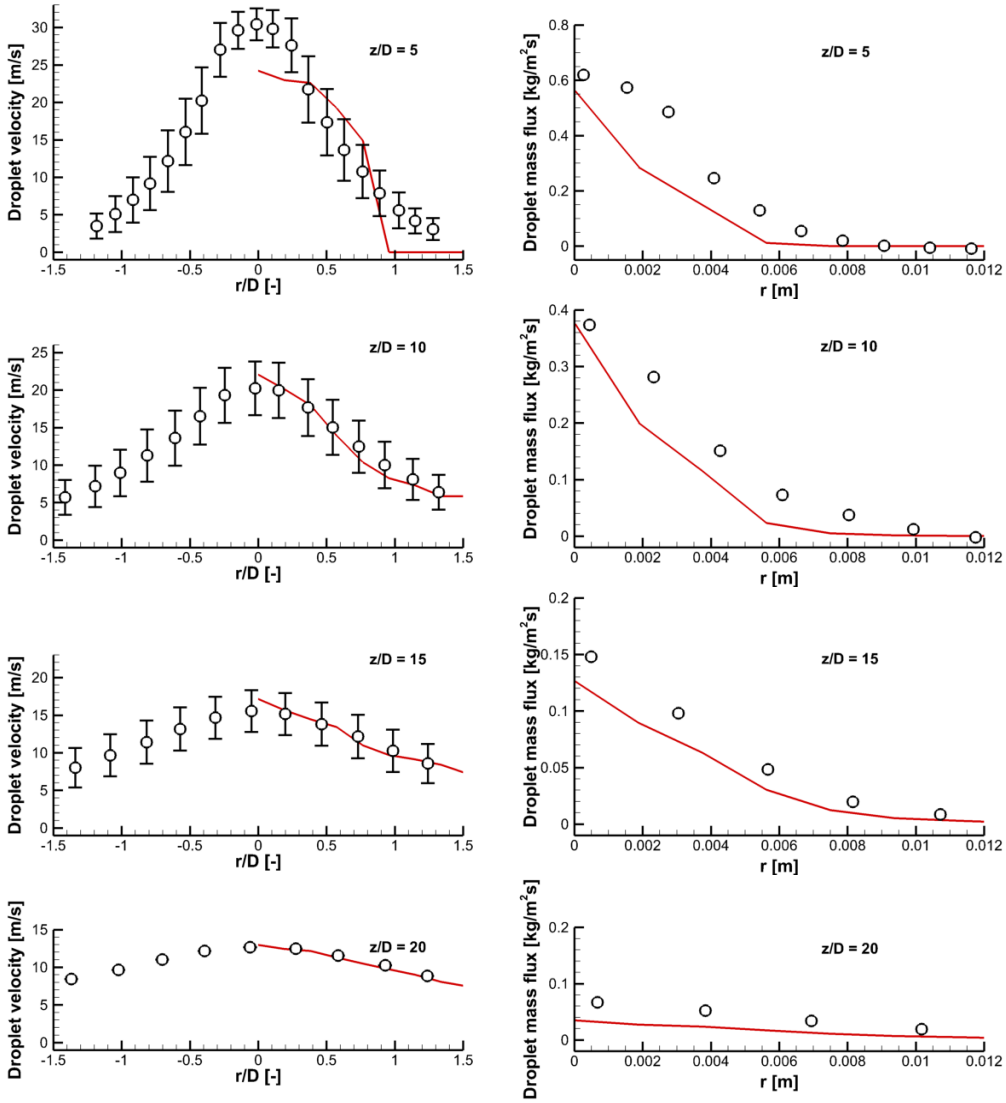

Fig. 14. Predicted and measured radial distributions of mean droplet velocity (left) and liquid mass flow rate (right) at different distances from the nozzle. Solid lines – Fire3D model (time-averaged data), symbols – measurements by Chen *et al.* [2006] (low speed, fine droplet spray LFS)

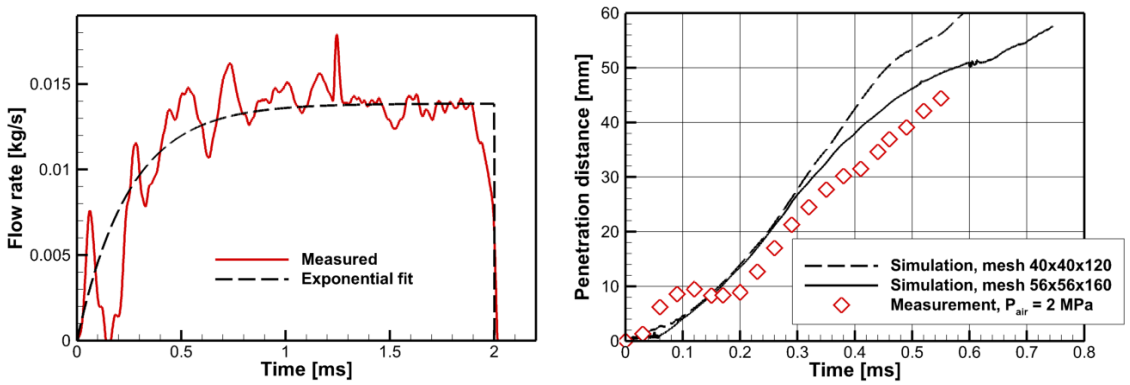

a) b)

Fig. 15. Diesel spray modelling: liquid injection mass flow rate (a) and spray tip penetration (b)

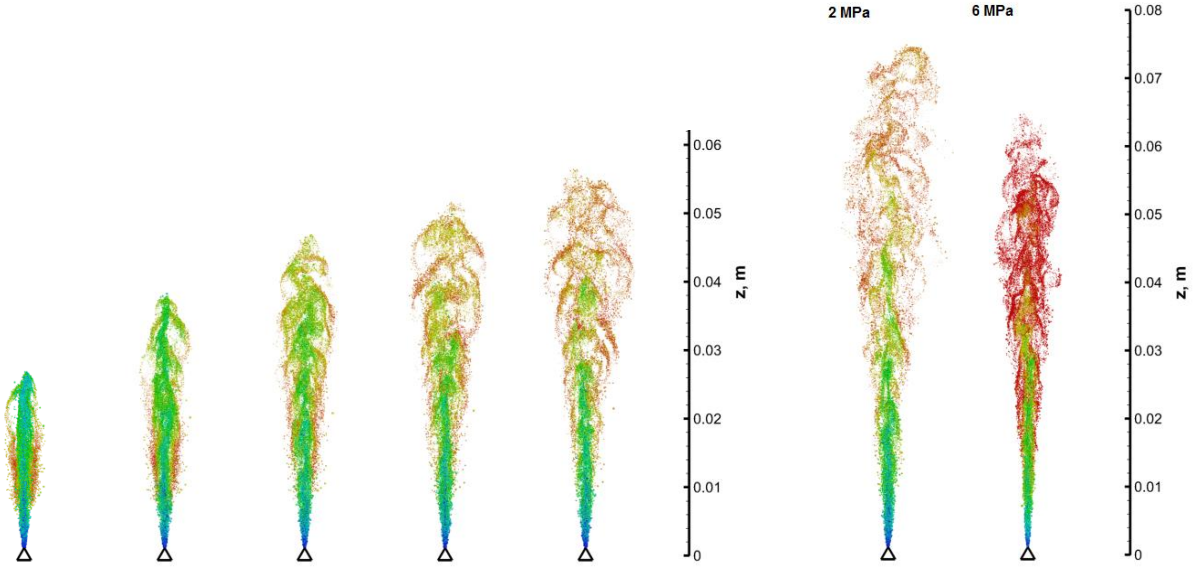

a) b)

Fig. 16. Predicted instantaneous droplet locations in axial plane of starting diesel spray: a) – gas pressure 2 MPa, time instants 0.3, 0.4, 0.5, 0.6 and 0.7 ms after start of injection; b) – time instant 0.9 ms after start of injection, gas pressure 2 and 6 MPa. Droplets are coloured by its temperature (400-472 K)

As shown in Fig. 15 (a), predicted propagation of spray tip correlates well with visible length of the starting spray observed in the experiments, and mesh refinement brings predictions closer to the measured data. Further spray development causes stabilization of the visible spray length, although vapour cloud propagates farther. Absence of the sharp spray edge obscures definition of the predicted spray length making it sensitive to the threshold droplet concentration which should be pre-assumed. In accordance with the experimental observations, spray edge propagates more slowly in a higher pressure environment. This is illustrated in Fig. 16 (b) which compares instantaneous droplet locations in the axial plane at the same time instant for two ambient pressures 2 and 6 MPa.

CONCLUSIONS

To allow for the internal temperature gradient, exact numerical or analytical solution of heat transfer equation inside evaporating droplet is a matter of choice when a single droplet is considered but is prohibitively expensive when a very large number of droplets is modelled in sprays. As a simple and yet sufficiently accurate alternative, two approximate approaches to predict surface temperature

(higher order polynomial approximation and the heat balance integral method) are proposed. These approaches have been implemented in the LES-based CFD spray model and included in Fire3D code.

A robust and computationally efficient numerical algorithm for solving inherently stiff equations of droplet heating and evaporation has been developed to meet the requirements of high-resolution spray models with large number of droplets. Stiffness of the equations stems from the disparity of two governing time scales corresponding to: (1) rapid droplet heating (or cooling) from the initial temperature to the equilibrium (wet bulb) temperature and (2) slow droplet evaporation at the equilibrium temperature. Robustness and computational efficiency of the proposed algorithm is achieved by use of unconditionally stable strongly implicit integration scheme and appropriate adaptation of the time step. The time step adaptation procedure identifies the relevant time scale to be resolved by comparing droplet surface temperature and the wet bulb temperature. After the initial phase of rapid heating or cooling is complete, the time step is increased to a value that is still sufficient to resolve droplet life time.

The spray model developed in this work has been applied to replicate three essentially different experimental scenarios in which turbulent sprays of water, acetone, and diesel fuel were investigated. Reasonable agreement has been demonstrated for predicted and measured droplet sizes and velocities as well as for the spray tip penetration dynamics. New numerical algorithms used to calculate surface temperatures of evaporating droplets with non-uniform internal temperature did not incur observable increase of CPU time in turbulent spray simulations.

ACKNOWLEDGEMENTS

This work is a part of research project «A universal spray model for engineering applications» funded by Russian Foundation for Basic Research (RFBR 10-08-92602-KO_a) and the Royal Society (JP090548), UK. Support by Gefest Ltd (St.-Petersburg) is gratefully acknowledged.

REFERENCES

Abramzon, B. and Sirignano, W.A. [1989], Droplet vaporization model for spray combustion calculations, *Int. J. Heat Mass Trans.* Vol. 32, No 9, pp. 1605-1618.

Aggarwal, S.K., Tong, A.Y. and Sirignano, W.A. [1984], A Comparison of Vaporization Models in Spray Calculations. *AIAA J.*, Vol. 22, No 10, pp. 1448-1457.

Balasubramanyam, M.S., Chen, C.P. and Trinh H.P. [2007], A New Finite-Conductivity Droplet Evaporation Model Including Liquid Turbulence Effect. *J. Heat Trans.*, Vol. 129, No 8, pp.1082-1086.

Balasubramanyam, M.S. and Chen, C.P. [2008], Modeling liquid jet breakup in high speed cross-flow with finite-conductivity evaporation. *Int. J. Heat Mass Trans.*, Vol. 51, No 15-16, pp. 3896-3905.

Bertoli, C., Migliaccio, M. [1999], A finite conductivity model for diesel spray evaporation computations. *Int. J. Heat Fluid Flow*, Vol. 20, No 5, pp. 552-561.

Bird R.B., Stewart W.E., Lightfoot E.N. [2002], *Transport Phenomena*, 2nd ed., Wiley, 895 p.

Chen, Y.-C., Starner, S.H. and Masri, A.R. [2006], A detailed experimental investigation of well-defined, turbulent evaporating spray jets of acetone, *Int. J. Multiphase Flow*, Vol. 32, No 4, pp. 389-412.

Dean, J.A. [1999], *Lange's handbook of chemistry*, 15th ed., NY: McGraw-Hill.

Dombrovsky, L.A. and Sazhin, S.S. [2003], A parabolic temperature profile model for heating of droplets, *ASME J. Heat Trans.*, Vol. 125, pp. 535-537.

Goodman, T.R. [1958], Heat balance integral and its application to problems involving a change of phase, *Trans. ASME. J. Heat Trans.*, Vol. 80, pp. 335-342.

Law, C.K. and Sirignano, W.A. [1977], Unsteady Droplet Combustion with Droplet Heating-II: Conduction Limit. *Combust. Flame*, Vol. 28, pp. 175-186.

Maqua, C., Castanet, G. and Lemoine, F. [2008], Bicomponent droplets evaporation: Temperature measurements and modeling, *Fuel*, Vol. 87, No 13-14, pp. 2932-2942.

Miller, R.S., Harstad, K. and Bellan, J. [1998], Evaluation of equilibrium and non-equilibrium evaporation models for many-droplet gas-liquid flow simulations, *Int. J. Multiphase Flow*, Vol. 24, No 6, , pp. 1025-1055.

Ra, Y., Reitz, R.D. [2009], A vaporization model for discrete multi-component fuel sprays, *Int. J. Multiphase Flow*, Vol. 35, No 2, pp. 101-117.

Reid, R.C., Prausnitz, J.M. and Poling, B.E. [1987], *The Properties of Gases and Liquids*, 4th ed., McGraw-Hill, 741 p.

Renksizbulut, M., Bussmann, M. and Li X. [1992], A Droplet Vaporization Model for Spray Calculations. *Particle & Particle Systems Charact.*, Vol. 9, No 1-4, pp. 59-65.

Sazhin, S.S., Abdelghaffar, W.A., Sazhina, E.M. and Heikal M.R. [2005], Models for droplet transient heating: effects on droplet evaporation, ignition and break-up. *Int. J. Therm. Sci.*, Vol. 44, No 7, pp. 610-622.

Sazhin, S.S. [2006], Advanced models of fuel droplet heating and evaporation, *Prog. Energy Comb. Sci.*, Vol. 32, No. 2, pp. 162-214.

Saznin, S.S., Martynov, S.B., Kristyady, T., Crua, C. and Heikal, M.R. [2008], Diesel fuel spray penetration, heating, evaporation and ignition: modelling vs. experimentation. *Int. J. Engineering Systems Modelling and Simulation*, Vol. 1, No. 1, pp. 1-19.

Sirignano, W.A. [1983], Fuel droplet vaporization and spray combustion theory. *Prog. Energy Combust. Sci.*, Vol. 9, No 4, pp. 291-322.

Sirignano, W.A. [2010], *Fluid Dynamics and Transport of Droplets and Sprays*, 2nd ed. Cambridge Univ. Press, 462 p.

Snegirev, A.Yu. [2004] Statistical Modelling of Thermal Radiation Transfer in Buoyant Turbulent Diffusion Flames. *Combust. Flame*, Vol. 136, No 1-2, pp. 51-71.

Snegirev, A.Yu. and Lipjainen, A.L. [2008], Modeling and Simulations of Fine Water Spray in Buoyant Turbulent Diffusion Flame. *Heat Trans. Res.*, Vol. 39, No. 2, pp. 133-149.

Snegirev, A., Lipjainen, A. and Talalov, V. [2010], Flame suppression by water sprays: flame-spray interaction regimes and governing criteria, *12th Int. conf. Interflam 2010 (Nottingham, UK, 5-7 July 2010)*. London: Interscience Comm., Vol. 1, pp. 189-199.

Snegirev, A.Yu., Sazhin, S.S., Talalov, V.A. and Savin, M.V. [2011], Validation study of the model to predict heating and vaporization of a liquid droplet, *Proc. SPbSPU Phys. Math. Sci. (Nauchno-tekhnicheskie Vedomosti SPbSPU)*, No 2(122), pp. 48-59 (In Russian).

Snegirev, A. and Talalov, V. [2012], An accurate and simple approach to allow for the transient temperature gradient in a vaporizing droplet, *ASME 2012 Fluids Engineering Division Summer Meeting FEDSM2012, Puerto Rico, USA, July 8-12, 2012* (submitted).

Subramanian, V.R., Ritter, J.A. and White R.E. [2001], Approximate Solutions for Galvanostatic Discharge of Spherical Particles: I. Constant Diffusion Coefficient, *J. Electrochem. Soc.*, Vol. 148, No 11, pp. E444-E449.

Subramanian, V.R., Diwakar, V.D. and Tapriyal D. [2005], Efficient Macro-Micro Scale Coupled Modeling of Batteries, *J. Electrochem. Soc.*, Vol. 152, No 10, pp. A2002-A2008.

Yuen, M.C., Chen, L.W. [1976], On drag of evaporating liquid droplets, *Comb. Sci. Tech.*, Vol. 14, pp. 147-154.

Yoon, S.S., Hewson, J.C., DesJardin, P.E., Glaze, D.J., Black, A.R. and Skaggs, R.R. [2004], Numerical modeling and experimental measurements of a high speed solid-cone water spray for use in fire suppression applications, *Int. J. Multiphase Flow*, Vol. 30, No 11, pp. 1369-1388.

Yoon, S.S., Kim, Ho Y. and Hewson, J.C. [2007], Effect of initial conditions of modeled PDFs on droplet characteristics for coalescing and evaporating turbulent water spray used in fire suppression applications, *Fire Safety J.*, Vol. 42, No 5, pp. 393-406.

Zeng, Y. and Lee, C.F. [2002], A model for multicomponent spray vaporization in a high-pressure and high-temperature environment, *J. Eng. Gas Turbines Power*, Vol. 124, No 3, pp. 717-724.